# Highly Active Metastable Ruthenium Nanoparticles for Hydrogen Production through the Catalytic Hydrolysis of Ammonia Borane

*Enass K. Abo-Hamed, Timothy Pennycook, Yana Vaynzof, Chris Toprakcioglu, Alexandros Koutsioubas, and Oren A. Scherman**

*Late transition metal nanoparticles (NPs) with a favorably high surface area to volume ratio have garnered much interest for catalytic applications. Yet, these NPs are prone to aggregation in solution, which has been mitigated through attachment of surface ligands, additives or supports; unfortunately, protective ligands can severely reduce the effective surface area on the NPs available for catalyzing chemical transformations. The preparation of 'metastable' NPs can readily address these challenges. We report herein the first synthesis of monodisperse metastable ruthenium nanoparticles (RuNPs), having sub 5 nm size and an fcc structure, in aqueous media at room temperature, which can be stored for a period of at least 8 months. The RuNPs can subsequently be used for the catalytic, quantitative hydrolysis of ammonia-borane (AB) yielding hydrogen gas with 21.8 turnovers per min at 25 °C. The high surface area available for hydrolysis of AB on the metastable RuNPs translated to an $E_a$ of 27.5 kJ mol$^{-1}$, which is notably lower than previously reported values for RuNP based catalysts.*

## 1. Introduction

Hydrogen is among the leading candidates as an alternative energy source for the future. Whilst hydrogen gas is used in a variety of ways to generate energy, the most efficient process entails its conversion to electrical energy via fuel cell technologies.[1] Fundamental technology exists for both the storage of hydrogen as well as its on-board production;[2] however, improvement of current methods is crucial to achieve more efficient practical applications. On account of its high hydrogen content (19.6 wt%), high stability under fuel cell reaction conditions, and non toxicity,[3] ammonia-borane (AB) meets the 2015 US Department of Energy (DOE) targets for a hydrogen resevoir of 9 wt% and 81 g L$^{-1}$.[4] As the catalytic hydrolysis of AB can in principle provide stoichiometric conversion to hydrogen gas at room temperature,[5,6] the development of an economic and efficient catalyst that operates under mild conditions is of paramount importance.[7]

Catalytic nanoparticles (NPs) have attracted a great deal of interest among both scientific and industrial communities owing to the unique properties derived from their characteristic large surface area-to-volume ratios.[8] In order to achieve their small size during preparation, and to prevent subsequent particle coalescence due to the enhanced surface tension associated with small particle sizes,[9,10] NPs

E. K. Abo-Hamed, Dr. O. A. Scherman
Melville Laboratory for Polymer Synthesis
Department of Chemistry
University of Cambridge
Lensfield Road, Cambridge CB2 1EW, UK
Tel: +44 1223 334370
E-mail: oas23@cam.ac.uk

Dr. T. Pennycook
Department of Materials
University of Oxford
Parks Road, Oxford OX1 3PH, UK
(b) SuperSTEM Laboratory
STFC Daresbury Campus
Keckwick Lane, Daresbury WA4 4AD, UK

Dr. T. Pennycook
SuperSTEM Laboratory, STFC Daresbury Campus
Keckwick Lane, Daresbury, WA4 4AD, UK

Prof. Y. Vaynzof
Centre for Advanced Materials (CAM)
Im Neuenheimer- Feld 227, 69120 Heidelberg, Germany

Prof. C. Toprakcioglu
Department of Physics
University of Patras
Patras 26500, Greece

Dr. A. Koutsioubas
Synchrotron Soleil, Beamline SWING
Sain Aubin BP48, F-91192 Gif Sur Yvette Cedex, France

DOI: 10.1002/smll.201303507

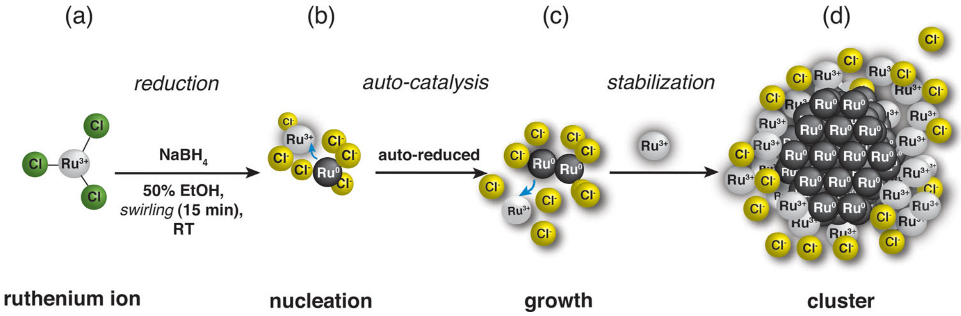

Figure 1. Formation of the metastable RuNP. a) Ruthenium ions in solution; b) nucleation, forming initial seeds upon introducing $NaBH_4$; c) growth of seed dimensions, which occur when further ruthenium ions are introduced to the formed nuclei, eventually leading to the final stable state; d) metastable cluster, when remaining ruthenium ions are no longer reduced.

are generally stabilized through the introduction of surfactants or surface-bound ligands and stabilizing agents.[11] While the NPs must be covered with protective ligands for the purpose of stability and to allow them to be used in catalytic applications, the presence of the same protective ligands can also reduce substrate accessibility on the catalytic NP surface. These competing factors have presented the synthetic chemist with a dilemma, as a compromise between these competing issues must be sought. We report herein the preparation of metastable ruthenium nanoparticles (RuNPs) through the reduction of $RuCl_3$ precursor with sodium borohydride. Our method not only offers versatility and simplicity in the preparation of organic ligand-free nanoparticles, but also allows for enhanced exposure of the catalytic surface of the NPs.

Ruthenium complexes are among the most widely studied materials due to their catalytic performance. Some ruthenium complexes have recently been shown to be effective in the hydrolysis of AB.[12–15] A number of different shapes, structures and compositions of RuNPs have also been investigated for their catalytic activity in a wide range of chemical transformations.[16–18] As the size of NPs has a marked effect on the overall catalytic activity,[19] their formation is of great consequence and is controlled by an aggregation process during reduction of the metal ions. In principle the particle size can be determined by influencing the relative rates of nucleation and cluster growth.[20] Traditionally, in order to achieve such stable aggregates on the nanometer scale, the formation process, has been carried out in the presence of stabilizing ligands. Aggregation kinetics have been evaluated using a classical Derjaguin, Landau, Verwey and Overbeek (DLVO) model, whereby the interaction between two particles is the sum of the electrostatic repulsions controlled by the NP surface potentials, and all of the interparticle van der Waals attractions are controlled by the Hamaker coefficient for the bulk metal. Particle collisions by Brownian motion give rise to substantial agglomeration, if repulsive interactions or stabilizing ligands are not present. However, according to Turkevich and co-workers, there are three reaction stages in forming metal NPs: (i) an initial nucleation step, followed by (ii) aggregation, and finally (iii) growth.[21]

## 2. Results and Discussion

The growth of the NPs to their final (stable) size is generally determined by the amount of stabilizing ligands present during reduction.[22–24] It has also been reported, that cluster growth stops only when all of the metal ion precursor has been consumed, with further growth only occurring by aggregation of small into large clusters; importantly, the relative rates for all of these steps are responsible for the resultant size of the NPs.[25] Watzky et al. suggest that an intermediate autocatalysis step occurs between steps (i) and (ii), where the surface of the nuclei acts to reduce proximate metal ions in solution.[26]

Metastable RuNPs were prepared in 1:1 (v/v) aqueous ethanol solution, where $NaBH_4$ was applied to reduce the $RuCl_3 \cdot H_2O$ precursor to the NPs, without further stabilizing additives and agents being employed. We hypothesized that instead of adding external stabilizing ligands, the aggregation process could be arrested in a quasi-reduced state, as metastable RuNPs, whereby a collection of both $Ru^{3+}$ and $Cl^-$ ions prohibit further agglomeration as illustrated in **Figure 1**. To examine our hypothesis, X-ray photoelectron spectroscopy (XPS) measurements were carried out on the metastable RuNPs 48 hours after reduction. **Figure 2** shows the C1s-Ru3d XPS spectrum of a 0.5 mM sample. The spectrum consists of two C1s peaks and Ru3d doublets; the low energy Ru3d doublet (Ru3d5 peak at binding energy of 280.4 eV) is assigned to $Ru^0$. XPS data therefore confirms that the RuNPs observed by TEM (Figure 4) consist of $Ru^0$. It was also found that only 19.04% of the Ru signal originates from $Ru^0$, while the remaining Ru originates from a high-energy Ru3d doublet (Ru3d5 peak at binding energy of 281.9 eV), which is assigned to $RuCl_3$. Additionally, C1s peaks at 285.6 eV (C-C) and 288.0 eV (C=O) are observed in the XPS. The initial concentration of $RuCl_3 \cdot H_2O$ played a decisive role in determining the final size of the RuNPs, (vide infra). In order to minimize possible side effects stemming from variations in temperature or differences in ionic strength on NP growth, varying concentrations of the metal precursor were used for the formation of RuNPs whilst keeping the reaction temperature and ionic strength, governed by the sodium borohydride reducing agent, constant. Borohydrides have a tendency to be adsorbed onto the surface of the NPs acting as ion sources during the

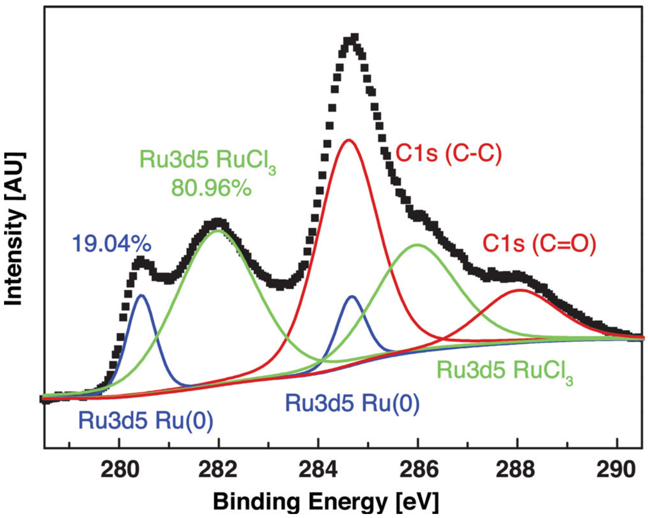

Figure 2. XPS spectra collected on metastable RuNPs in solution (0.5 mM).

growth step.[27] As the covalent ruthenium-chloride bonds break in the $RuCl_3$ precursor, electrostatic repulsions arise and a competition develops between all free ions in solution for their adsorption onto the NP surface. After all the borohydride ions are consumed and oxidized to the corresponding borates, the remaining ruthenium ions likely serve as the main stabilizing agent giving rise to the metastable NPs.

To further understand the stability of the RuNPs in solution, small angle X-ray scattering (SAXS) measurements were carried out. **Figure 3** a shows the SAXS pattern of a 1 mM metastable RuNP solution. The scattering curve is dominated by a strong correlation peak that exhibits a maximum at $q_{max} = 0.00796$ Å$^{-1}$. Although correlation peaks can appear in interacting systems without necessarily implying the existence of a special correlation distance, it is nevertheless of interest to compare the spacing ($2\pi/q_{max}$) suggested by the position of the peak, to the mean distance between the NPs. Therefore, the mean distance between the NPs arising from the SAXS data is 79 nm. However, a rough estimate for the same distance can be calculated from the concentration of the NPs in solution. TEM results indicate that the mean diameter of RuNPs prepared from a 1 mM $RuCl_3\cdot H_2O$ solution is approximately 1.2 nm (see Figure 3c). Assuming a spherical shape, it is possible to estimate the average distance between NPs in solution. Thus, for a 1 mM sample (which has a total concentration of dispersed metallic ruthenium of 0.2 mM and NP volume fraction of ca. $1.6 \times 10^{-6}$) the mean distance between NPs is calculated to be roughly 83 nm, which is commensurate with the spacing (79 nm) associated with the peak position. The inset of Figure 3b shows SAXS patterns that correspond to a series of samples obtained by consecutive dilutions of the original 1 mM sample composition. As can be seen, the correlation peak shifts slightly to lower q-values but persists at least up to a dilution by a factor of 16, while obscuring the underlying form factor of the NPs and preventing reliable extraction of the particle radius from the scattering data. The presence of a prominent correlation peak at such a low volume fraction of the dispersed phase is indicative of the strong electrostatic repulsion experienced by the charged NPs. The long range of the inter-particle repulsion implied by the data can be attributed to the fact that the NPs must be highly charged. This observation would also account for the remarkable stability of the RuNPs despite the absence of any added protective ligand on the NP surface in this system. It is indeed noteworthy that the SAXS spectrum of a 1 mM solution, when measured again after 30 days, was found to be identical to the original spectrum, within experimental error, demonstrating the lack of any significant structural changes in the system over this timescale.

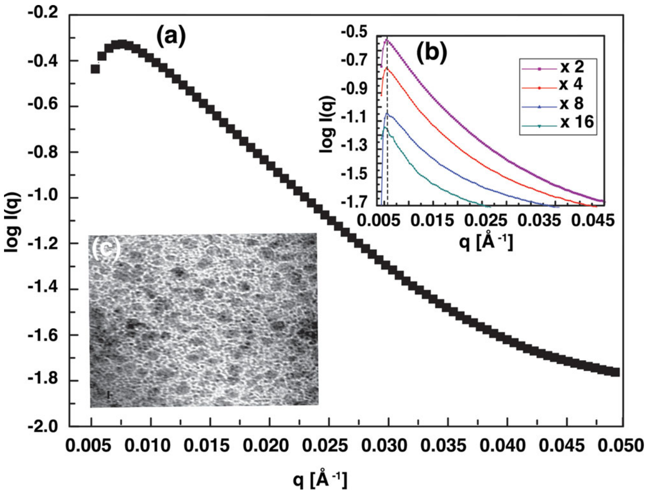

Figure 3. a) Small angle scattering profile of a 1 mM metastable RuNP solution. b) SAXS patterns associated with a series of samples obtained by consecutive dilutions of the original composition. c) TEM image of a 1 mM metastable RuNPs solution.

One of the key problems that could emerge from the absence of stabilizing ligands over time is the loss of consistent NP shape and structure on account of agglomeration. To examine this, transmission electron microscopy (TEM) and aberration corrected high angle annular dark field scanning transmission electron microscopy (HAADF STEM) were conducted to characterize the particle size distribution and structure. A number of solutions of RuNPs varying in concentration and aged for 24 hours were deposited on holey carbon grids for the purpose of this analysis. Representative TEM micrographs are presented in **Figure 4** and the analysis of their corresponding size distribution is shown in Figure 4f with all of the corresponding raw data in Figure S1 (Supporting Information). One trend is readily apparent: as the precursor concentration increases, there is a concomitant decrease in the average particle size of the RuNPs from 2.76 nm (for 0.3 mM) to 0.97 nm (1.1 mM). Additionally, as the precursor concentration is increased (see TEM images in Figure 4a–e) there is a progressive increase in the appearance of sub-nm ‘seeds’. Moreover, there is a marked difference in appearance from Figure 4c, where the majority of the NPs are larger, to Figure 4d where there appears to be a co-existence of both large and much smaller ‘seed’ particles. Thus, when the precursor concentration reaches 0.9 mM and above, the NP growth process appears to be shortened at the expense of the seeding step. This implies that a competition between the over abundance

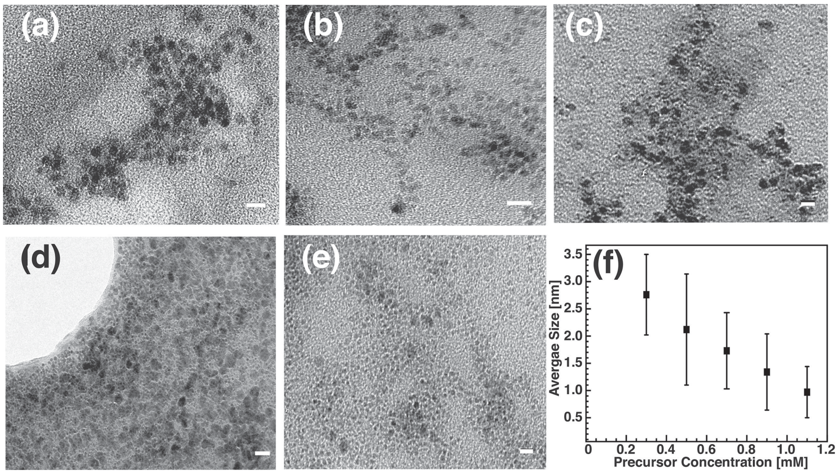

**Figure 4.** TEM images of metastable RuNPs where initial concentration of precursor used is: (a) 0.3 mM, (b) 0.5 mM, (c) 0.7 mM, (d) 0.9 mM and (e) 1.1 mM. Scale bars = 5 nm. (f) Plot of initial precursor concentration vs. RuNP average size distribution obtained by counting at least 200 NPs.

of seed particles develops during the growth step if the particles are partially stabilized by borohydride ions on the surface.

To gain further insight into the atomic structure of the metastable RuNPs, samples were subjected to HAADF STEM analysis. The images obtained show that despite the lack of stabilizing ligands, freestanding RuNPs are indeed formed (see Figure S2d, Supporting Information) and possess a face centred cubic (fcc) structure viewed down the <110> direction as shown in **Figure 5** with a horizontal lattice spacing of 2.75 Å and a lattice constant of approximately 3.9 Å. Agglomerations of particles were also observed; however, these often took the form of several nanocrystals (NCs) with small areas of their surfaces in contact with one another, nevertheless maintaining a relatively high area of exposed nanocrystalline surface (see Figure S2a–c, Supporting Information). Furthermore, these agglomerated particles appeared to possess the same fcc crystal structure when aligned with the electron beam. To the best of our knowledge, the first and only fcc structure as a nanoparticle phase observed so far was reported recently by Kitagawa *et al.*[28] Interestingly, it was observed that the fcc structure was obtained only when a precursor of Ru(acac)$_3$ was applied in the presence of a poly(N-vinyl-2-pyrrolidone) stabilizing agent. In comparison, our method realizes RuNPs with an fcc structure for the first time using $RuCl_3{\cdot}H_2O$ as a precursor in aqueous media, where there are no added stabilizing agents or supports.

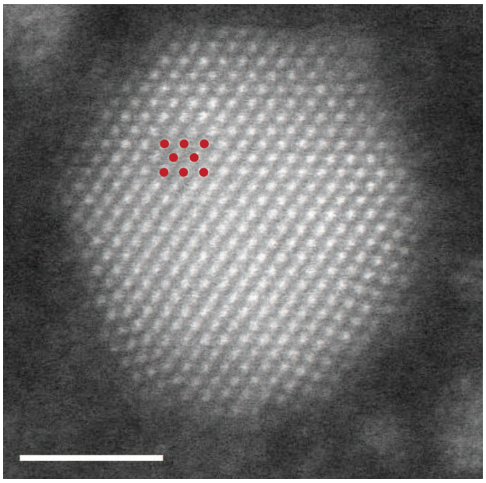

**Figure 5.** HAADF STEM image of a fcc structured (red circles) RuNP obtained from 0.3 mM initial concentration of precursor, scale bar = 2 nm.

In the absence of stabilizing agents, the weakly-coordinating chloride anions do not provide enough stabilization for the metal NPs;[29] therefore, the Ru$^{3+}$ ions remaining in solution must play an important role in both the overall NP growth process and in the surface stabilization of the final clusters, forming part of the 'protecting' layer. As more 'protecting' ions are available at higher initial concentration of the precursor, the observation that smaller particles exist at higher concentrations corresponds well with this explanation, as a constant amount of reducing agent was applied across this series. When the concentration of borohydride ions decreases over the course of metal reduction, it was expected that the stability of the the formed particles would also decrease with time as a partial stabilizing agent was consumed consistent with previous suggestions.[30] However, in our case, the notable long-term stability observed for the metastable RuNPs after all borohydride is consumed, might be attributed to the large amount of Ru$^{3+}$ ions still present in solution. The presence of these ions was confirmed by XPS, and correlates well with the SAXS data reflected by the maintained interparticle distance enhanced by electrostatic repulsion.

In addition to testing the effect of precursor concentration on NP size and stability, several other variables were tested for their contribution to particle stability in solution, including agitation and the type of alcohol used in the aqueous solution. Varying the alcohol from ethanol to either methanol or propanol was found to be ineffective and reduced the overall NP stability, while a 1:1 (v/v) water:ethanol mixture was found to be the best composition. When a magnetic stir bar was used during reduction, the stability of the produced NPs was remarkably decreased; the stir bar serves as a nucleation surface, which accelerated aggregation to larger particles and eventually led to precipitation. In stark contrast, when gentle *swirling* was applied during metal reduction with a bench-top incubator, RuNPs of a controllable size were formed and exhibited enhanced stability for more than 8 months. In synthetic methods reported in the literature, the ligands employed limit the catalytic surface available for chemical transformation, thereby necessitating ligand removal and subsequent growth in particle size or surface oxidation.[31,32] In contrast, our method provides a metastable approach towards the formation of high surface area RuNPs, thus potentially offering a general route for the synthesis of long-term ion-stabilized NPs in the absence of typical organic or inorganic ligands with control over size.

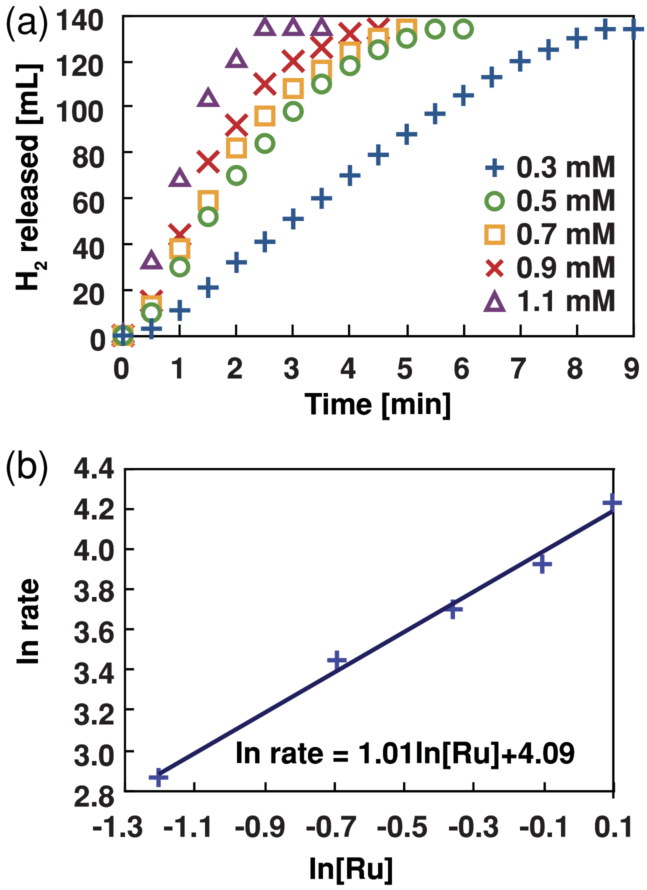

**Figure 6.** a) Plot of time vs. volume of hydrogen generated from AB hydrolysis by 0.3–1.1 mM metastable RuNPs at room temperature ([AB] = 200 mM). b) Plot of hydrogen generation rate vs. the concentration of Ru, both in logarithmic scale.

As the high surface area RuNPs displayed long-term stability in aqueous media, they were particularly attractive for the catalytic hydrolysis of ammonia borane in water.[33] In order to establish the rate law for the hydrolysis of AB by our metastable RuNPs, the as-synthesized RuNPs were introduced to aqueous solutions of AB at 25 °C with a very low stirring rate. For every 10 mL of AB solution (2 mmol, 200 mM) added to a 10 mL dispersion of RuNPs, the $H_2$ gas evolved from the hydrolysis reaction was collected in a buret and measured every minute. To ensure that the gas formation consisted solely of hydrogen and did not contain any ammonia *via* the direct decomposition of AB, the gas produced was tested by an acid-base titration. Variation of RuNP concentration, reaction temperature and AB concentration were all tested to elucidate an AB hydrolysis kinetic profile.

To examine the effect of RuNP concentration on the hydrolysis reaction, five different concentrations (0.3, 0.5, 0.7, 0.9 and 1.1 mM) were chosen such that they were identical to those previously investigated in the $RuCl_3$ reduction (see Figure 4f). **Figure 6**a shows a plot of the volume of $H_2$ gas produced as a function of time. The rate of hydrogen generation was directly determined from a linear fit of the data. For all five concentrations, a stoichiometric amount of $H_2$ (6 mmol) was generated in a rapid manner. The $H_2$ evolution rate increased with catalyst concentration as clearly seen in Figure 6b. Thus, a higher rate of reaction was achieved for smaller, more active NPs on account of the overall surface area to volume ratio for the NP solution. Moreover, a double logarithmic plot of hydrogen generation rate as a function of catalyst concentration (Figure 6b) yields a slope of 1.01, strongly indicative of a first-order hydrolysis reaction.

The effect of the AB substrate concentration on hydrolysis was also investigated by carrying out the reaction with different AB concentrations of 50, 100, 150 and 200 mM, while keeping the the RuNP concentration constant at 0.5 mM. Here, $H_2$ gas generation was found to be independent of the AB concentration (see Supporting Information, Figure S3a). Figure S3b (Supporting Information) shows the double logarithmic plot of $H_2$ as a function of AB concentration with a slope of 0.06, confirming that the 2.2 nm RuNPs (produced at 0.5 mM), is roughly zero-order with respect to the AB concentration. The zero-order rate dependency highly suggests that AB adsorption onto the surface of the RuNP catalysts is a rate-limiting step.[34]

Finally, the catalytic hydrolysis of AB by the metastable RuNPs was carried out at different temperatures. In order to determine the activation energy, $E_a$, for the hydrolysis reaction, a 200 mM solution of AB was subjected to the 0.5 mM RuNPs over a temperature range of 25–45 °C. **Figure 7**a shows the plot of $H_2$ gas produced as a function of time monitored for five different temperatures (25, 30, 35, 40 and 45 °C). The

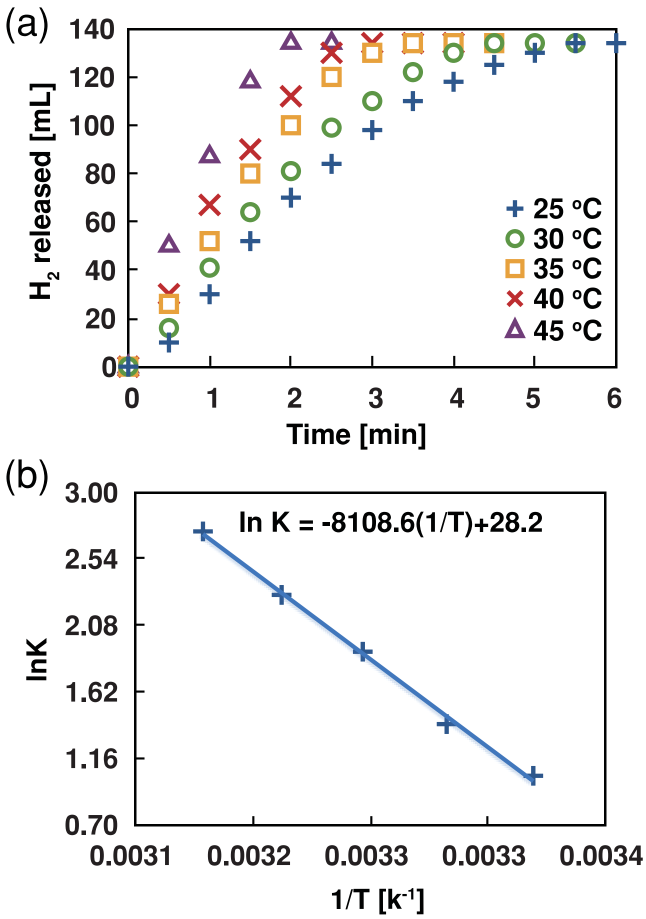

**Figure 7.** a) Plot of time vs. volume of hydrogen gas generated from AB hydrolysis by 0.5 mM metastable RuNPs at room temperature ([AB] = 200 mM). b) Arrhenius plot.

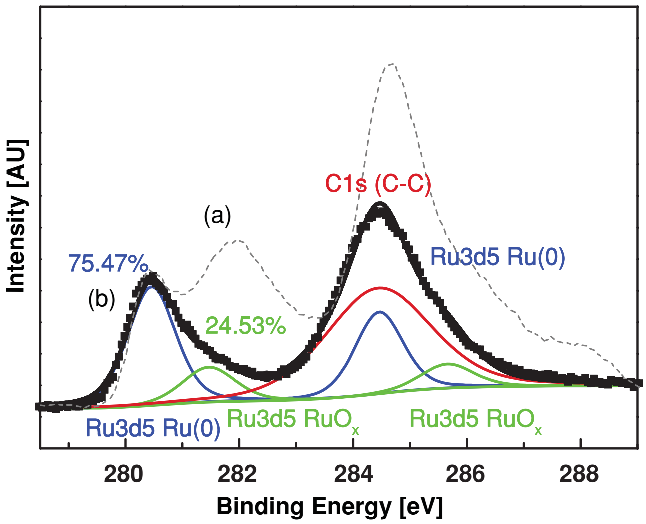

**Figure 8.** XPS spectra of the same 0.5 mM RuNPs sample (a) before (- - dashed line), and (b) after completion of a complete hydrolysis of 2 mmol AB ( — solid line).

**Table 1.** $H_2$ generation from aqueous AB catalysed by Ru-based catalysts.

| entry | catalyst | particle size (nm) | $E_a$ (kJ mol$^{-1}$) | ref |
|---|---|---|---|---|
| 1 | Ni-Ru alloy NPs | 9 | 37 | [12] |
| 2 | PSSA-co-MA[a)]<br>Ru(0) nanoclusters | 1.9 | 54 | [36] |
| 3 | laurate-Ru(0) nanoclusters | 2.6 | 47 | [37] |
| 4 | Ru nanolusters/C | 1.7 | 34.81 | [38] |
| 5 | Ru(0)NPs-$H_2PO_4$ | 2.9 | 92.4 | [39] |
| 6 | Ru/C | – | 76 | [16] |
| 7 | RuNPs/MCNT[b)] | 2.5 | 33 | [17] |
| 8 | Ru @ $Al_2O_2$ | 2.5 | 48 | [40] |
| 9 | metastable RuNPs | 2.2 | 27.5 | this study |

[a)] PSSA-*co*-MA=poly(4-styrenesulfonic acid-*co*-maleic acid) stabilized; [b)] Ruthenium(0) nanoparticles supported on multiwalled carbon nanotubes.

rate constants were derived from the linear part of the plot for each temperature, and were used to calculate the $E_a$ of 27.5 kJc·mol$^{-1}$ from the Arrhenius plot shown in Figure 7 b. The catalytic performance of the RuNPs could be further characterized by the turnover frequency (TOF), which was calculated to be 21.8 mol $H_2$·(mol catalyst c· min)$^{-1}$.

Interestingly, the metastable RuNPs remained in solution during the entire hydrolysis of the AB (2 mmol) substrate. To further investigate the oxidation state of the NPs after a full catalytic cycle, a dispersion of RuNPs (0.5 mM) was isolated and subjected to XPS. **Figure 8** displays the XPS spectra both prior to (dashed line) and after (solid line) the hydrolysis reaction. The spectrum after a full catalytic cycle consists of two Ru3d doublets and a single C1s peak (285.5 eV). The doublet at 280.4 eV (as before catalysis Figure 8 a), is assigned to $Ru^0$; however, the $Ru^0$ peak contributes to over 75% of the Ru signal (Figure 8 b) after a complete cycle. Moreover, we do not observe any evidence for $Ru^{3+}$ or $Cl^-$ in the sample. As no protective ligands are attached to the NPs and the protective $Ru^{3+}$ ions no longer surround the NPs, a contribution from an oxidized Ru species (Ru3d5 peak at 281.4 eV) was observed, which has likely occurred during sample preparation (in air).[35]

**Table 1** lists the particles sizes and activation energies for the previous reports on AB hydrolysis catalyzed by ruthenium species in comparison to our method reported here. While we have not quite achieved the smallest RuNP species reported (see Table 1 entries 4 vs. 9), the $E_a$ for our metastable NPs is substantially less than any previously reported Ru-based system. Moreover, our metastable RuNPs are simple to prepare and remain stable in solution without any support.

## 3. Conclusion

Our report represents the first example whereby RuNPs are stabilized without protective organic ligands or additional supports while simultaneously exhibiting a high catalytic activity. We have demonstrated a simple yet efficient method to prepare metastable RuNPs in a 1:1 (v/v) water:ethanol mixture. The preparation process was concentration dependent on the $RuCl_3$·$H_2O$ precursor with respect to control over the NP size. Despite the lack of a conventional organic or inorganic stabilizing ligands present on the NP surface, metastable RuNPs were shown to be stable for many months likely on account of surrounding $Ru^{3+}$ ions, the presence of which was confirmed by XPS. Moreover, a consistent interparticle distance between the NPs in solution was readily observed by SAXS measurements; we believe, that this is attributed to the repulsion forces arising from these surrounding ions. Thus, the highly charged NP surfaces appear to gain long-term stability and control over size through charge-charge repulsion as opposed to direct ligand attachment. Additionally, the metastable RuNPs exhibit an fcc structure and were shown to be a promising catalytically active material for production of $H_2$ through the hydrolysis of ammonia-borane in water at room temperature. The activation energy of 27.5 kJ mol$^{-1}$ for the catalytic hydrolysis was found to be remarkably low and resulted in a turnover number of 21.8 per minute, rendering the metastable RuNPs as an extremely promising candidate for the production of hydrogen gas under mild conditions for practical applications.

## 4. Experimental Section

*Chemicals*: $RuCl_3$·$H_2O$, $NaBH_4$ (99.99%), ammonia-borane (97%) and all solvents used were purchased from Sigma-Aldrich and used as received.

*General Metastable RuNP Preparation*: Stock solution of 30 mM $RuCl_3$·$H_2O$ in distilled water was first prepared and sonicated for 20 min. To a conical flask, 40 mL of 1:1 (v/v) aqueous ethanol was added and different amounts of 0.012, 0.02, 0.028, 0.036 and 0.044 mmol of a stock solution was added to obtain specific concentrations (0.3, 0.5, 0.7, 0.9 and 1.1 mM, respectively). The solution was sonicated for 1 min and 1 eq of (0.1 M) $NaBH_4$ of 1:1 (v/v) aqueous ethanol was immediately added with swirling for 15 min using a bench-top incubator at 300 rpm at room temperature. The colour of the solution was immediately changed from light to dark brown. The solution was left to age for 24 h.

*Hydrolysis of AB by Metastable RuNPs*: The catalytic activity of metastable RuNPs for the hydrolysis of AB was evaluated by measuring the rate of hydrogen generation produced in a conventional water-filled gas burette set-up. Prior to starting the catalytic activity test, a jacketed reaction flask (25 mL) containing a Teflon-coated stir bar was placed on a magnetic stirrer and thermostated to 25.0 (±) 1 °C by circulating water through its jacket from a constant temperature bath. Then, a burette filled with water was connected to the reaction flask to measure the volume of the hydrogen gas released from the reaction mixture. A 10 mL dispersion of RuNPs was loaded into the reaction flask and 64 mg (2 mmol) $NH_3BH_3$ (corresponding to generation of a maximum 6 mmol equivalet to134 mL $H_2$ gas at 25.0 (±) 1 °C and 0.91 atm pressure) was added into the catalyst solution under 800 rpm stirring rate. The volume of hydrogen gas evolved was measured by recording the displacement of water level every 30 s. A $^{11}B$ NMR spectrum of the solution after one day showed only the signals attributed to metaborate at 9 ppm.

*Characterization*: Transmission electron microscopy (TEM) characterization was carried out by a FEI Philips Tecnai 20 TEM under an accelerating voltage of 200 kV. Samples were prepared by applying one drop of the as-prepared dispersion onto a Holey®carbon coated copper TEM grid (300 mesh).

High angle annular dark field (HAADF) images were acquired on a Nion UltraSTEM 100, operated at 100 kV, equipped with a cold field emission electron source and a corrector capable of neutralizing up to fifth order aberrations.[41]

$^{11}B$ NMR spectra were recorded on a BRUKER Avance 500MHz spectrometer operating at 160.48 MHz.

*Photoemission spectroscopy*: The PES samples were transferred to the ultrahigh vacuum (UHV) chamber (ESCALAB 250Xi) for XPS measurements. XPS measurements were carried out using a XR6 monochromated Alk$\alpha$ X-ray source (hv = 1486.6 eV) with a 650 µm spot size and a pass energy of 20 eV.

SAXS experiments were performed at the SWING beamline of the French synchrotron facility SOLEIL. The x-ray wavelength ($\lambda$ = 1.03 Å) and sample-detector distance (D = 3000 mm) corresponded to a scattering wavevector range of $0.004$ Å$^{-1}$ $< Q <$ $0.35$ Å$^{-1}$. The solvent and solutions were filled into a thin-walled diameter quartz capillary that was inserted in a vacuum chamber, so that the whole beam path remained under vacuum conditions. Scattering data (40 frames of duration for each sample) were then collected with a low-noise AVIEX CCD detector. The 2D scattering images were radially averaged, divided by the transmitted intensity and finally averaged for each sample. The scattering curves that correspond to the nanoparticle form and structure factor were obtained by subtracting the solvent scattering signal.

## Supporting Information

*Supporting Information is available from the Wiley Online Library or from the author.*

## Acknowledgements

*The authors wish to acknowledge Dr Samuel Jones, Anna Andreou and Emma-Rose Janecek for valuable discussions. This work was supported by an ERC Starting Investigator Grant (ASPiRe, 240629) and an ESPRC Programme grant (sNaP, EP/G060649/1). STEM experiments were performed at SuperSTEM, the EPSRC UK national facility for aberration-corrected STEM.*

[1] S. M. Haile, *Acta Mater.* **2003**, *51*, 5981–6000.
[2] L. Schlapbach, A. Züttel, *Nature* **2001**, *414*, 353–358.
[3] O. Metin, V. Mazumder, S. Özkar, S. Sun, *J. Am. Chem. Soc.* **2010**, *132*, 1468–1469.
[4] S. Satyapal, C. Read, G. Ordaz, G. Thomas, *2006 Annual DOE Hydrogen Program Merit Review: Hydrogen Storage*, US Department of Energy, Washington, DC, **2006.**
[5] M. Chandra, Q. Xu, *J. Power Sources* **2006**, *156*, 190.
[6] F. H. Stephens, V. Pons, R. T. Baker, *Dalton Trans.* **2007**, 2613–2626.
[7] F. H. Stephens, R. T. Baker, M. H. Matus, D. J. Grant, D. A. Dixon, *Angew. Chem.* **2007**, *119*, 760–763.
[8] G. C. Bond, *Surf. Sci.* **1985**, 966–981.
[9] M. Zahmakiran, S. Özkar, *Appl. Catal. B* **2009**, *89*, 104–110.
[10] R. Narayanan, M. A. El-Sayed, *J. Am. Chem. Soc.* **2003**, *125*, 8340–8347.
[11] P. Xi, F. Chen, G. Xie, C. Ma, H. Liu, C. Shao, J. Wang, Z. Xu, X. Xud, Z. Zeng, *Nanoscale* **2012**, *4*, 5597–5601.
[12] G. Chen, S. Desinan, R. Rosei, F. Rosie, D. Ma, *Chem. Eur. J.* **2012**, *18*, 7925–7930.
[13] B. B. L. Conley, D. Guess, T. J. Williams, *J. Am. Chem. Soc.* **2011**, *133*, 14212–14215.
[14] N. Blaquiere, S. Diallo-Garcia, S. I. Gorelsky, D. A. Black, K. Fagnou, *J. Am. Chem. Soc.* **2008**, *130*, 14034–14035.
[15] M. Käß, A. Friedrich, M. Drees, S. Schneider, *Angew. Chem. Int. Ed.* **2009**, *48*, 905–907.
[16] S. Basu, A. Brockman, P. Gagare, Y. Zheng, P. Ramachandran, W. Delgass, J. Gore, *J. Power Sources* **2009**, *188*, 238–243.
[17] S. Akbayrak, S. Özkar, *ACS Appl. Mater. Interfaces* **2012**, *4*, 6302–6310.
[18] G. P. Rachiero, U. B. Demirci, P. Miele, *Catal. Today* **2011**, *170*, 85–92.
[19] C. K. Rhee, B.-J. Kim, C. Ham, Y.-J. Kim, K. Song, K. Kwon, *Langmuir* **2009**, *25*, 7140–7147.
[20] J. S. Bradley, B. Tesche, W. Busser, M. Maase, M. T. Reetz, *J. Am. Chem. Soc.* **2000**, *122*, 4631–4636.
[21] J. Turkevich, P. C. Stevenson, J. Hillier, *Faraday Discuss. Soc.* **1951**, *11*, 55.
[22] D. V. Leff, P. C. Ohara, J. R. Heath, W. M. Gelbart, *J. Phys. Chem.* **1995**, *99*, 7036–7041.
[23] T. Teranishi, M. Hosoe, T. Tanaka, M. Miyake, *J. Phys. Chem. B* **1999**, *103*, 3818–3827.
[24] M. Hostetler, J. Wingate, C.-J. Zhong, J. Harris, R. Vachet, M. Clark, J. Londono, S. Green, J. Stokes, G. Wignall, G. Glish, M. Porter, N. Evans, R. Murray, *Langmuir* **1998**, *14*, 17–30.
[25] T. Tanaka, J. Ohyama, K. Teramura, Y. Hitomi, *Catal. Today* **2012**, *183*, 108–118.
[26] M. A. Watzky, R. G. Finke, *Chem. Mater.* **1997**, 3083.
[27] D. L. V. Hyning, C. F. Zukoski, *Langmuir* **1998**, *14*, 7034–7046.
[28] K. Kusada, H. Kobayashi, T. Yamamoto, S. Matsumura, N. Sumi, K. Sato, K. Nagaoka, Y. Kubota, H. Kitagawa, *J. Am. Chem. Soc.* **2013**, *135*, 5493–5496.
[29] S. Özkar, R. G. Finke, *J. Am. Chem. Soc.* **2002**, *124*, 5796–5810.
[30] D. L. Van Hyning, W. G. Klemperer, C. F. Zukoski, *Langmuir* **2001**, *17*, 3120–3127.
[31] L. Wen, J.-K. Fu, P.-Y. Gu, B.-X. Yao, Z.-H. Lin, J. Z. Zhou, *Appl. Catal. B* **2008**, *79*, 402–409.
[32] H. Yin, Z. Ma, M. Chi, S. Dai, *Catal. Lett.* **2010**, *136*, 209–221.
[33] M. Yadav, Q. Xu, *Energy Environ. Sci.* **2012**, *5*, 9698–9725.

[34] D. Sun, V. Mazumder, O. Metin, S. Sun, *ACS Nano* **2011**, *5*, 6458–6464.
[35] K.-W. Park, J.-H. Choi, B.-K. Kwon, S.-A. Lee, Y.-E. Sung, *J. Phys. Chem. B* **2002**, *106*, 1869–1877.
[36] O. Metin, S. Sxahin, S. Özkar, *Int. J. Hydrogen Energy* **2009**, *34*, 6304–6313.
[37] F. Durap, M. Zahmakiran, S. Özkar, *Int. J. Hydrogen Energy* **2009**, *34*, 7223–7230.
[38] H. Liang, G. Chen, S. Desinan, R. Rosei, F. Rosie, D. Ma, *Int. J. Hydrogen Energy* **2012**, *37*, 17921–17927.
[39] S. Casliskan, M. Zahmakiran, F. Durap, S. Özkar, *Dalton Trans.* **2012**, *41*, 4976–4984.
[40] H. Can, O. Metin, *Appl. Catal. B* **2012**, *125*, 304–310.
[41] O. Krivanek, G. Corbin, N. Dellby, B. Elston, R. Keyse, M. Murfitt, C. Own, Z. Szilagyi, J. Woodruff, *Ultramicroscopy* **2008**, *108*, 179–195.

Received: November 12, 2013